Journal of Constructional Steel Research 219 (2024) 108788

Contents lists available at ScienceDirect

Journal of Constructional Steel Research

journal homepage: www.elsevier.com/locate/jcsr

Out-of-flatness of steel plate girder webs, Part II: Shear strength and behavior

Parfait M. Masungi [a,*], Maria E.M. Garlock [a], Kevin E. Augustyn [b], Spencer E. Quiel [b]

[a] Princeton University, Dept. of Civil and Environmental Engineering, 54 Olden Street, Princeton, NJ 08544, USA
[b] Lehigh University, Dept. of Civil and Environmental Engineering, 117 ATLSS Drive, Bethlehem, PA 18015-3176, USA

ARTICLE INFO

Keywords:
Steel plate I-girders
Initial imperfections
Shear strength
Finite element analysis
Web shear buckling
Web shear mechanism

ABSTRACT

This paper presents a series of validated finite element (FE) models geared to parametrically examine the effects of initial web out-of-flatness imperfections on the shear strength and behavior of steel plate girders under pure shear. The prototype girder models are based on field measured imperfection shapes and magnitudes, with variations in web slenderness (93, 109, and 118) and panel aspect ratio (0.89, 2.02, 2.22, and 2.29). Additional model cases are analyzed by incorporating idealized eigenmode shapes and scaled to web out-of-flatness tolerance limits per AASHTO/AWS D1.5. The FE strength results are compared against various code-based nominal shear strength predictions. The following key findings are derived: (1) field measured and eigenmode imperfections exhibit similar shear behavior and deformation response throughout all shear mechanism stages; (2) the yield mechanism of a stiffened web panel in shear is negligibly impacted by the initial imperfections of the web and is triggered by second-order flexural bending from in-plane shear-induced compression; (3) an initial imperfection with an eigenmode shape and a maximum magnitude ranging from *d/300* to *d/600* (where *d* equals to the least panel dimension) can suitably approximate the shear strength of plate girders when compared with field measured imperfections; and (4) code-based nominal shear strength predictions demonstrate to be conservative for web panel aspect ratios $\geq$2.0.

1. Introduction

Deep I-shaped steel plate girders are formed by welding a vertical web plate between the upper and lower flange plates as shown in Fig. 1. By reducing the web thickness (t_w) and increasing the web depth (D), structural designers can often improve the efficiency of the material usage and increase flexural stiffness. The web plates are often slender and therefore susceptible to shear buckling, resulting in permanent out-of-plane deformation. Previous research has demonstrated that slender web plates have additional strength beyond their elastic limit, known as the postbuckling capacity [1]. To resist web shear buckling and enhance their postbuckling strength, transverse (i.e. vertical) stiffeners are intermittently welded onto the web between the flanges to create stiffened web panels with a longitudinal dimension a (Fig. 1b). [2,3].

As illustrated in Fig. 1c, the slender web plate will develop "out-of-flatness" initial imperfections due to the fabrication, forming, welding, and assembly of the plate girder. These out-of-flatness shapes can have one or more waves, and the maximum magnitude may not be located at the center of the panel [4]. To be clear, the term "*out-of-flatness*" is typically used to define the web deformations that result from fabrication (before service loads are applied). In this study, the term "*initial imperfection*" will be used to denote the local out-of-plane distortions that are imposed on the web plate as an initial condition for nonlinear finite element (FE) analysis. Essentially, both terms (out-of-flatness and initial imperfection) refer to the same deformations but are used in different contexts (field measurements in actual girders versus numerical models of those girders, respectively).

Code-based predictive equations for calculating the nominal postbuckling shear capacity in slender webs [5–8] do not quantify the impact of the magnitude and shape of initial imperfections. Rather, the postbuckling theories upon which those code-based equations focus on the development of tension field action (TFA) in the web and engagement of the stiffeners and flanges to resist the shear force [6,9]. However, previous research has shown that the shape and magnitude of initial imperfections can influence the maximum shear capacity (V_{max}) of stiffened web panels [10–14]. Standards such as the American Welding Society (AWS) specifications [15], AWS D2.0–66 [16], AASHTO/AWS D1.5 [17], and other international standards [18–26]

* Corresponding author.
E-mail addresses: pmasungi@princeton.edu (P.M. Masungi), mgarlock@princeton.edu (M.E.M. Garlock), seq213@lehigh.edu (S.E. Quiel).

https://doi.org/10.1016/j.jcsr.2024.108788
Received 10 February 2024; Received in revised form 14 May 2024; Accepted 16 May 2024
Available online 28 May 2024

impose out-of-flatness tolerance limits on the measured web imperfections of fabricated plate girders. These standards define the out-of-flatness limits as a function of d, which is the lesser of web panel dimensions a and D (see Fig. 1b). Zhang [10] performed an extensive review of these standards and concluded that web out-of-flatness tolerance limits have little-to-no theoretical or engineering basis. Rather, these limits are imposed on the basis of aesthetics (especially for the visible webs of fascia girders) as well as general assumptions regarding the deleterious impact of large imperfections on structural behavior.

As noted, previous research has shown that the shape and magnitude of initial imperfections can influence the maximum shear capacity (V_{max}) of stiffened web panels [10–14]. In particular, Bergfelt [27] studied the influence of factors such as slenderness, and initial imperfection shape and magnitude on the shear strength of web plates. The imperfection shapes used were all eigenmodes. Results showed that the web will develop lower shear strength if the initial imperfection shape has the same shape as the buckling eigenmode shape. Conversely, if the initial imperfection shape deviates from that of the buckling eigenmode shape, then the web shear strength would likely increase. Other researchers used an idealized or theoretical web initial imperfection shape to propose strength reduction factors for web out-of-flatness as a function of the web slenderness [28,29]. Note that none of these studies mentioned considered field measured imperfection shapes and magnitudes.

The authors conducted a detailed review of existing measurement approaches and code-based tolerance limits for web out-of-flatness imperfections in welded plate girders. In addition, field measurements capturing the out-of-flatness of web plates were performed on 12 plate girders with depths ranging from 0.914 to 2.08 m at a major steel bridge fabrication facility in Pennsylvania, USA [4]. Each measured plate girder had stiffened web panels (defined as having length a) that were bounded by transverse stiffeners. From the 12 girders, data was collected for 23 individual web panels (defined by the ratio a/D). The maximum web out-of-flatness imperfection magnitude on each web panel had the following characteristics: (1) collectively, the measured web panels had a mean magnitude value of $d/170$ with a standard deviation of $d/108$; (2) the location of the maximum web out-of-flatness imperfection was localized, covering a small area like large 'dimples'; (3) the maximum point of out-of-flatness did not always correspond with the center point of the web panel; and (4) the out-of-flatness shapes were not idealized sinusoids but could be more approximated as having single, double, or triple waves out-of-plane [4].

This paper builds upon the companion field study conducted by the authors [4] to further numerically examine the maximum shear capacity and behavior of plate girder webs with out-of-flatness shapes and magnitudes based on the aforementioned field measurements. The results of the FE models implemented those realistic measured web out-of-flatness imperfections as an initial condition. Consequently, these results were compared against FE models for which the imposed web initial imperfections were based on an idealized eigenmode with maximum magnitude scaled to code-based tolerance limits. Finally, the obtained shear strength values from the FE models were evaluated and assessed against code-based nominal shear strength predictions per the American Institute of Steel Construction (AISC) 360–22 [30] and Eurocode 3 (EC 3) [18] specifications.

2. Generalized web shear response

Recent research by the authors has demonstrated that second order flexural bending, developed via in-plane compression of the out-of-plane deformed plate, in a buckled web under shear will combine with tension field stresses to induce plasticity and a resulting shear failure mechanism [31]. The shape and magnitude of initial imperfections of a web plate will therefore play an important role in determining the maximum shear capacity (V_{max}) of slender webs.

As discussed previously in Section 1, the shear behavior of web plates has been studied extensively via testing and numerical analysis for over 50 years [9,32,33]. Research produced during that period has led to the development of design models and equations for predicting the post-buckling shear strength and understanding the shear mechanics [6,9,33–36]. Recent experimental work by Scandella et al. [37] observed three phases of shear response, which were classified as linear elastic behavior (phase 1), stage 1 postbuckling behavior (phase 2), and stage 2 postbuckling behavior (phase 3). These three phases form the basis, with some modifications as provided in Fig. 2, which illustrates three stages in the shear mechanism response of slender I-shaped plate girders [31,38], which are discussed in the subsequent sections.

2.1. Stage 1: Elastic behavior

Linear elastic behavior (Stage 1) is depicted by the blue portion of the curve plotted in Fig. 2. Stage 1 ends when the elastic limit, V_{el}, is reached. At this point, the tensile stresses along the tension diagonal interact with the compression-induced second-order flexural bending stresses to produce a von Mises yield condition on the surface of the web plate. At V_{el}, this surface yield condition is connected diagonally across the tension field and emerges over the band where tensile stresses are largest due to second-order flexural bending (i.e. at the outer surface of the largest "bulge" of out-of-plane deformation). For clarity, it is important to specify that V_{el} is not equivalent to the elastic critical buckling load, V_{cr}, obtained via an elastic eigenvalue buckling analysis. Research by the authors [31] and others [37,39] has indicated that V_{cr} is simply a theoretical value to relate a bifurcation condition that is actually not accurately observed in any testing of webs in shear. Rather,

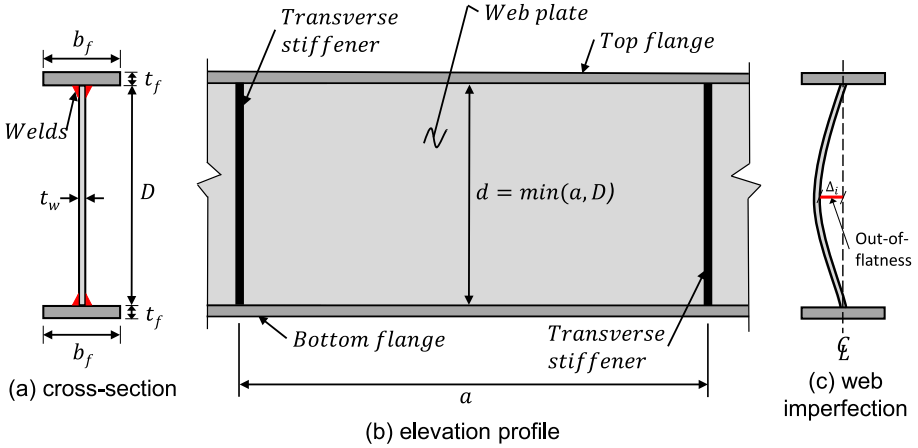

Fig. 1. Illustration of a typical I-shaped steel plate girder with a stiffened web.

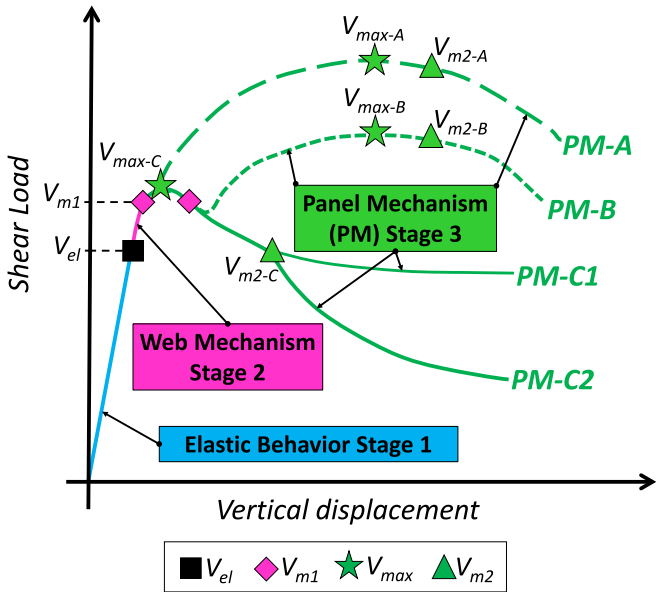

Fig. 2. Generalized shear mechanism response of stiffened web panels that undergo shear buckling.

the shear load-displacement response loses stiffness slowly (not abruptly) due to the initial imperfections and resulting second order bending of the deformed web plate.

2.2. Stage 2: Web mechanism

The web mechanism formation (Stage 2) is depicted by the magenta portion of the curve in Fig. 2. Beyond V_{el}, the in-plane shear stiffness will progressively decrease through Stage 2 as the surface yield condition begins to saturate (i.e. penetrate) through the full thickness of the web plate across the tension field diagonal (again, where compression-induced second-order flexural bending stresses are high). At the end of Stage 2, the web across the tension diagonal has achieved *von Mises yielding through the full thickness*. V_{m1} thereby represents the formation of the *web mechanism* (i.e. the first mechanism). During Stage 2, the stiffener and flange anchorage load paths are not significantly engaged since the web continues to provide significant shear resistance until V_{m1} is reached [31,38].

2.3. Stage 3: Panel mechanism

The panel mechanism (Stage 3) is depicted by the green solid and dotted lines in Fig. 2. Following the formation of the web mechanism, the plastified web panel will increasingly engage the bounding flange and stiffener plates, which now offer a stiffer load path than the web to support the applied shear load redistribution as the in-plane shear displacement progresses at an increasing rate. During stage 3, the maximum shear capacity, V_{max} occurs when the shear stiffness of the web plate reaches zero. Beyond V_{max}, the panel enters a slightly negative stiffness since the stiffeners and flanges may not provide significant shear resistance to the plastified web to enable hardening. Load redistribution to the flange and stiffener plate will cause a *panel mechanism* (i.e. the second mechanism) to develop past V_{max} at V_{m2}, when the load paths thru those elements yield or become unstable. The shear resistance of the stiffened web panel beyond V_{m2} will then proceed along a descending branch toward plastic hinge formations in the flanges and/or stiffeners, progressing toward the collapse of the panel.

The differences between PM-A, PM-B, PM-C1, and PM-C2 in stage 3 are attributed to the variation in the degree of support setup, boundary conditions, and the size of the boundary elements (flanges and stiffeners) [31]. For the paths marked PM-A and PM-B, the boundary elements are stiff enough to enable a slight amount of panel hardening past the formation of the web mechanism, such that that $V_{max} > V_{m2} > V_{m1}$. PM-A would be enabled by relatively stiff boundary elements that attract load path redistribution soon after the web mechanism is reached. PM-B exhibits a recovery of hardening stiffness once the boundary elements are engaged. In PM-C1 and PM-C2, the shear resistance decreases after Stage 2 and demonstrates a load path redistribution to boundary elements that are insufficiently stiff to enable subsequent hardening past the formation of the web mechanism [31]. PM-C1 develops an asymptotic descending branch once the boundary elements are engaged, while PM-C2 shows a more rapid descent toward collapse due to relatively weaker boundary elements.

2.4. Defining shear capacity: V_{m1} versus V_{max}

Various aspects of this 3-stage progression have been observed in numerous prior studies [6,28,38,40,41]. It is important to note that the magnitude of V_{max} is always greater than V_{m1}, but the increase depends on the sizing of the flange and stiffener plates as well as the initial out-of-flatness imperfections in the web. For example, V_{max-C} is only slightly greater (typically 1–2%) than V_{m1}, but V_{max-A} and V_{max-B} can be 5–12% greater than V_{m1} due to hardening enabled by the load redistribution to the boundary elements during Stage 3. Via parametric numerical analyses, Augustyn et al. [31,38] noted that increases or decreases in flange thickness could induce a corresponding increase or decrease in V_{m1} up to $\pm$10% by increasing the shear stiffness of the stiffened web panel, though most cases showed <5% change in V_{m1}.

Once the web mechanism has formed, other studies have shown that the flanges become increasingly engaged in localized weak-axis bending to anchor the tension field diagonal in the buckled web panel [33,37,41–43]. Scandella et al. [37] and Augustyn et al. [31] noted that this higher degree of flange engagement only emerges during Stage 3 once the web plate is fully plastified through its thickness along the tension diagonal. Furthermore, previous work by the authors [14,38] has demonstrated that flange stresses increase significantly after V_{max} toward the development of the panel mechanism at V_{m2}, at which point the web panel had entered the descending branch of its shear-displacement behavior.

The evaluation of flange engagement on the web and panel mechanisms (and the associated magnitudes of V_{m1}, V_{m2}, and V_{max}) is beyond the scope of this paper, which instead focuses on the impact of web out-of-flatness imperfections on these shear-displacement milestones. In particular, the results of the parametric FE analysis are used in this study to make a clear distinction between V_{max} as the maximum shear capacity and V_{m1} as the plastic postbuckling shear capacity.

3. Numerical modeling methodology

3.1. Dimensions and boundary conditions

As previously stated, a companion paper by the authors [4] presented field measurements of web out-of-flatness imperfections for 12 plate girders, where each web was composed of "panels" of length a that were bounded by transverse stiffeners. From the 12 girders, data was collected for 23 web panels (defined by a/D). This research study selected five of the 12 field measured plate girders, and from those five girders, 11 web panels formed the data set for the FE study presented in this paper. The selected plate girder webs were classified as noncompact sections ($D/t_w > 90$) with panel sections where $a/D \leq 3.0$ in order to consider the tension field action (TFA) per AISC specifications [30]. Table 1 provides the dimensions and measured imperfections of this data set which is used to conduct the parametric FE analyses using ABAQUS 2022 [44].

The FE modeling procedure and cross-sectional geometry in Fig. 3

Table 1
Field measurements from five newly fabricated plate girders, obtained in Part I of this study [4].

Plate Girder	Web			Flange			Panels			
	D (m)	t_w (mm)	D/t_w	b_f (mm)	Top t_{f1} (mm)	Bottom t_{f2} (mm)	a (m)	a/D	Segment	Max. Imp. Mag.
G1W	1.78	19.1	93	610	31.8	44.5	1.58	0.89	1	$d/255$
									2	$d/244$
									3	$d/183$
									4	$d/507$
G3W	1.88	15.9	118	511	50.8	57.2	3.80	2.02	1	$d/198$
									2	$d/188$
G4W	2.08	19.1	109	511	38.1	44.5	4.77	2.29	1	$d/241$
									2	$d/190$
G5W	2.08	19.1	109	511	41.3	44.5	4.62	2.22	1	$d/108$
									2	$d/96$
G6W	2.08	19.1	109	514	38.1	44.5	4.62	2.22	1	$d/120$
									Mean	$d/212$
									St. Dev.	$d/107$

Note: d denotes the least panel dimension between D or a.

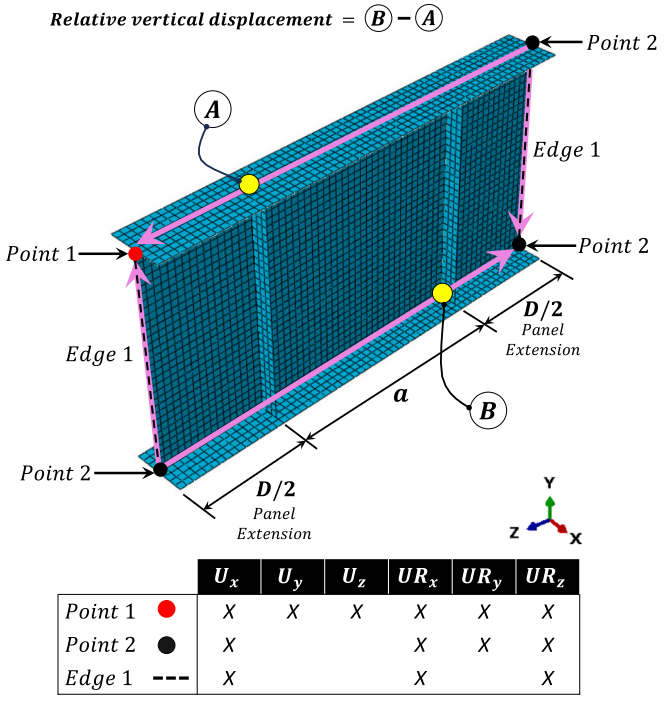

Fig. 3. Boundary conditions with pure shear edge loading on the panel extension FE models ("U" denotes translational restraint and "UR" denotes rotational restraint).

were based on the "panel extension" modeling approach by Wang et al. [14], which was validated against sixteen different test results to capture the maximum shear capacity and load path mechanics for stiffened webs in I-shaped plate girders. The welded interfaces between the web, flange, and stiffener plates were modeled using nodal tie constraints. The stiffener plate dimensions were not recorded during the field study; therefore, the stiffener plates for all models were designed to meet the area and inertia requirements of AISC guidelines [30], assuming a constant stiffener plate thickness of 19 *mm*. The resulting stiffener widths varied from 15 *cm* for G1W and G3W to 20 *cm* width for G4W, G5W, and G6W, respectively.

The boundary conditions and applied forces shown in Fig. 3 are applied directly to the web plate and not the stiffening elements. Uniformly distributed shear edge loads were applied along all four edges of the web as shown in Fig. 3, thus providing a pure shear condition. The steel material model used for the FE investigation had an elastic Young's modulus, $E = 200\ GPa$ ($\sim 29,000\ ksi$); a minimum yield stress, $F_y = 345\ MPa$ ($\sim 50\ ksi$); and Poisson's ratio, $\nu = 0.3$. The steel plates were modeled as elastoplastic with strain-hardening defined per EC3, Part 1–2 [45] provisions for hot-rolled steel plate. ABAQUS shell elements of type S4 [44] were utilized with 7 integration points through the plate thickness. The typical mesh global size had a 40 *mm* maximum edge dimension and was based on a convergence study performed by the authors for previous studies on the elastic buckling load of web panels [46]. The FE models did not include residual stresses – since previous work by the authors and others had demonstrated that residual stresses have negligible effect on the maximum shear capacity when validating numerical models against large-scale test results [14,31,38].

As mentioned, both the field measured and eigenmode imperfection shapes were used in the numerical study. These initial imperfections were imposed on the web plate nodes of the FE model prior to performing a nonlinear Modified Riks analysis. Field measured shapes were based on the contours presented in the companion work (Part I) [4], and scaled adequately as discussed in the subsequent sections. The numerical FE eigenmode imperfection shapes were obtained using a preliminary elastic critical eigenvalue "buckle" analysis of the extended panel model in ABAQUS, for which the maximum magnitude is described as a unit distance. The shapes were then scaled to the desired maximum magnitude and used as the initial condition for the nonlinear Modified Riks analysis.

3.2. Web imperfection parameters

This section discusses the web out-of-flatness imperfection parameters investigated in this research study. It is worth noting that going forward the term 'imperfection' will be employed to indicate the 'web out-of-flatness imperfection.' In Section 4, the shear mechanism response of web plates is numerically examined based on the following two imperfection parameters: *initial imperfection shape* (using field measured web shapes, or eigenmodes) and *initial imperfection magnitude* (using field measured values and code-based tolerance limits). As shown in Table 2, the initial imperfection shape and magnitude varied among the prototype web panels resulting in an extensive parametric set. The imperfection magnitude is described as a fraction of d, representing the least panel dimension, between D or a as done by the standards that set out-of-flatness limits (see Fig. 1) [4]. The parametric set was subdivided into two categories: The first category was comprised of those with *measured imperfections* (shapes and magnitudes as measured in the field, per Table 1). The second category included models with *tolerance imperfections* per design guidelines and tolerance limits as defined by the AASHTO/AWS D1.5 bridge welding code [17]. The second category employed the first and second positive eigenmodes for their shape with maximum magnitudes set equal to $d/67$ and $d/115$ representing the

Table 2
Shear milestones of FE models with various initial imperfections versus code-based shear strength predictions

Plate Girder	Model Type	Imperfection Shape	Imperfection Magnitude	FE Models V_{el} (kN)	FE Models V_{m1} (kN)	FE Models V_{max} (kN)	AISC without TFA V_n (kN)	AISC with TFA $V_{n.TFA}$ (kN)	EC3 without flange $V_{bw.Rd}$ (kN)	EC3 with flange $V_{b.Rd}$ (kN)
G1W	Measured Imperfection	Field – Panel 1	$d/255$	5997	6512	6514	6702	6908	5570	6074
		Field – Panel 2	$d/244$	5875	6430	6508				
		Field – Panel 3	$d/183$	5852	6297	6305				
		Field – Panel 4	$d/507$	6290	6621	6630				
	Tolerance Imperfection	1st eigenmode	$d/115$	4508	5765	5914				
		1st eigenmode	$d/67$	4080	5490	5652				
		2nd eigenmode	$d/115$	4457	5706	5769				
		2nd eigenmode	$d/67$	4348	5389	5444				
G3W	Measured Imperfection	Field – Panel 1	$d/198$	3734	4364	4390				
		Field – Panel 2	$d/188$	4293	4408	4408				
	Tolerance Imperfection	1st eigenmode	$d/115$	3181	4102	4102				
		1st eigenmode	$d/67$	3083	3919	3920				
		2nd eigenmode	$d/115$	3145	4090	4090				
		2nd eigenmode	$d/67$	2991	3862	3882				
G4W	Measured Imperfection	Field – Panel 1	$d/241$	5370	5749	5840	4853	5189	4988	5191
		Field – Panel 2	$d/190$	5071	5820	5935				
	Tolerance Imperfection	1st eigenmode	$d/115$	4152	5381	5402				
		1st eigenmode	$d/67$	3959	5134	5140				
		2nd eigenmode	$d/115$	4208	5499	5503				
		2nd eigenmode	$d/67$	3940	5210	5235				
G5W	Measured Imperfection	Field – Panel 1	$d/108$	5471	5930	6017	4879	5257	5002	5245
		Field – Panel 2	$d/96$	5496	5921	6039				
	Tolerance Imperfection	1st eigenmode	$d/115$	4182	5440	5451				
		1st eigenmode	$d/67$	4001	5183	5187				
		2nd eigenmode	$d/115$	4226	5538	5541				
		2nd eigenmode	$d/67$	3978	5245	5268				
G6W	Measured Imperfection	Field – Panel 1	$d/120$	5010	5924	6005	4879	5257	5002	5213
	Tolerance Imperfection	1st eigenmode	$d/115$	4179	5436	5440				
		1st eigenmode	$d/67$	3996	5177	5178				
		2nd eigenmode	$d/115$	4229	5523	5526				
		2nd eigenmode	$d/67$	3968	5246	5252				

largest allowable for stiffened web panels per [17]. Fig. 4 shows the contours of initial out-flatness imperfections (shapes and magnitudes) obtained from the eigenvalue buckle analysis. The first and second positive eigenmode shapes are shown with a consistent maximum initial imperfection equal to $d/67$ for contrast. The field measured initial imperfections shown in Fig. 5 as applied to the FE models of the extended panel models are shown with their respective maximum magnitudes for consistency and clarity. When comparing the eigenmode and field shapes of Fig. 4 and Fig. 5, it is observed that field measured imperfections have irregular patterns and do not coincide with the eigenmode shapes as concluded in part 1 [4].

Additional model cases were analyzed to enable a direct evaluation of the effects of initial imperfection shape and magnitude – the results of those models will be discussed in the next sections. The results listed under the FE Models, AISC, and EC3 columns in Table 2 will also be discussed in later sections.

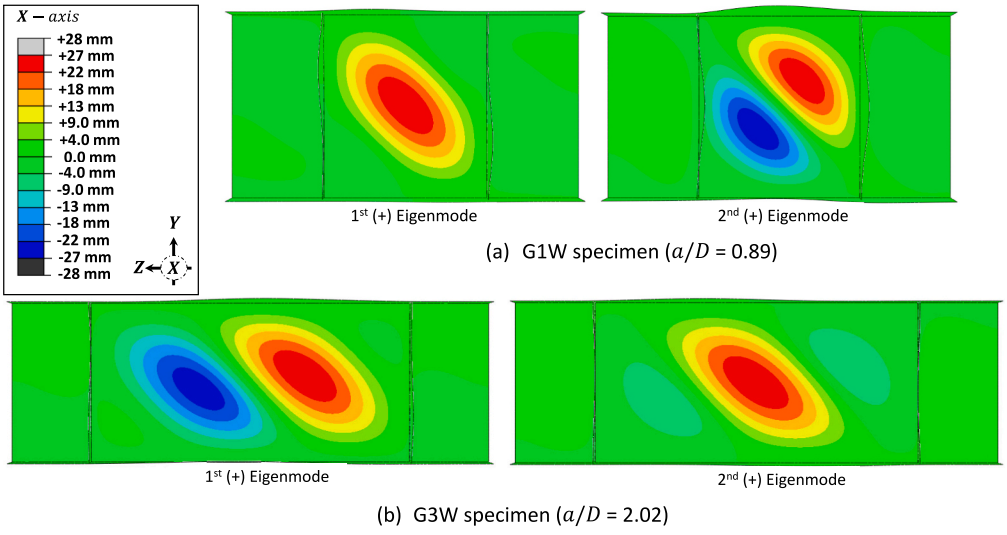

Fig. 4. Initial imperfections based on FE eigenmodes and scaled to a maximum magnitude of $d/67$.

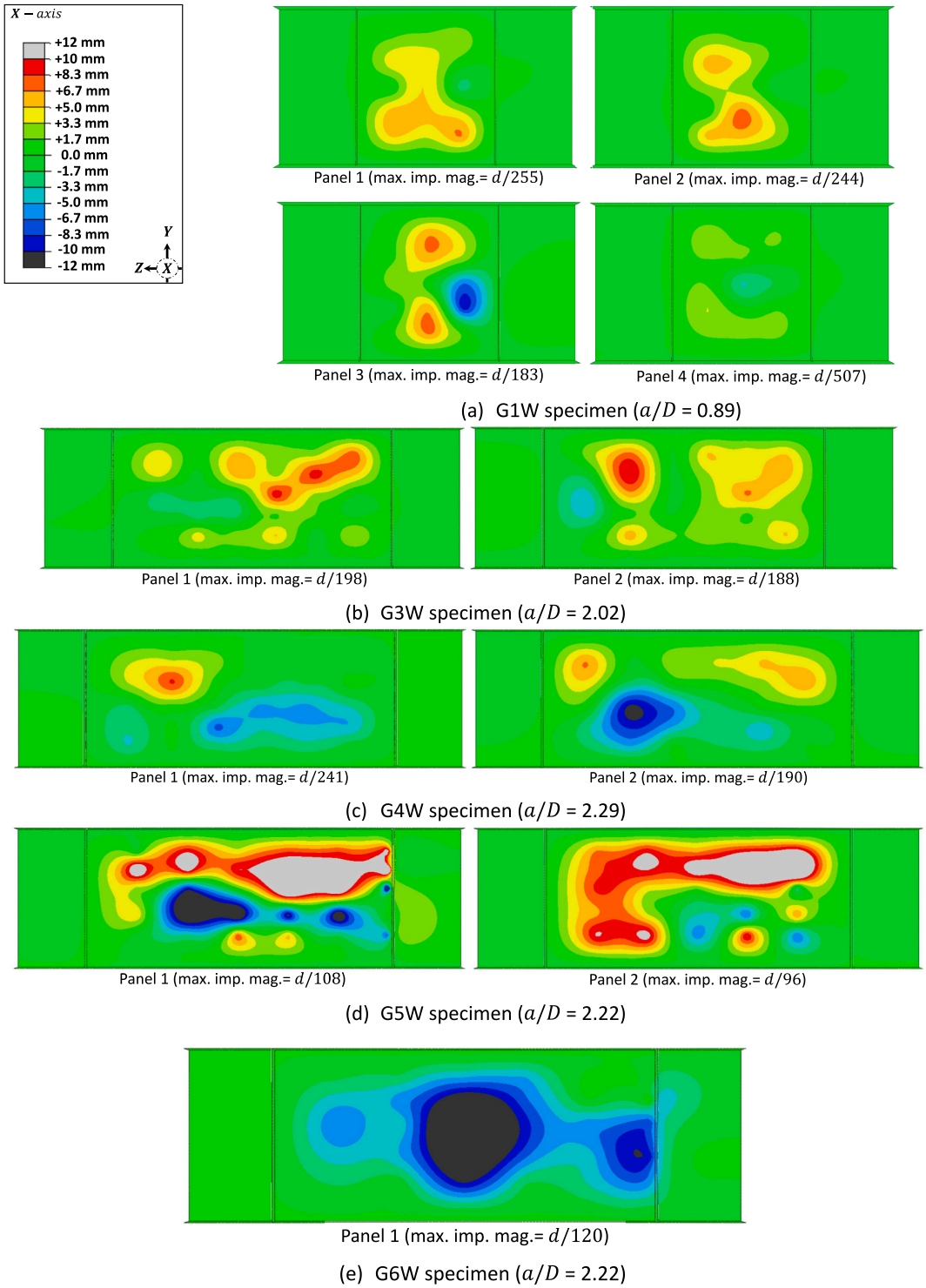

Fig. 5. Initial imperfections obtained from field measurements

In the results described in the next section, the "relative vertical displacement" (δ) is measured as the displacement of point B minus the displacement of point A on the extended panel model (see Fig. 3). Section 2 of this paper has defined the shear load milestones V_{el}, V_{m1}, V_{m2}, and V_{max}. Table 2 lists the value of each milestone as obtained from the finite element results. The method by which the shear milestones are identified is as follows [31]:

- V_{el} is the shear load at which the web plate has developed its first connected band of von Mises yielding on its surface across the tension diagonal. Again, this band coincides with the surface of peak tension stress (i.e. at the out-of-plane bulges shown at the elastic limit) from compression-induced second-order bending of the deformed shape. The in-plane shear stiffness of the panel is marginally impacted since the web plate has only just begun to experience partial yielding.
- V_{m1} is the shear load when the web plate first develops von Mises yielding through its full thickness in connected bands across the tension diagonal. Stresses from the tension field action and the compression-induced second-order bending have now combined to

induce a thru-thickness saturation of von Mises yielding, thus signifying a significant reduction of in-plane shear stiffness at the "web mechanism".

- V_{max} is the maximum shear capacity achieved for each FE analysis. It is at this point that the shear stiffness (which is taken as the derivative of the shear load over the relative vertical displacement) of the plastified web is zero.

The shear load at which the plastified web has engaged the bounding stiffeners and flanges to develop the "panel mechanism (V_{m2}) is not evaluated in this study due to the limitations of the panel extension model. The panel extension model is highly sensitive to the stiffness and load path redistribution of the web panel during the panel mechanism stage 3, and can only provide partial continuity from the adjacent panel and the boundary elements (flanges and transverse stiffeners).

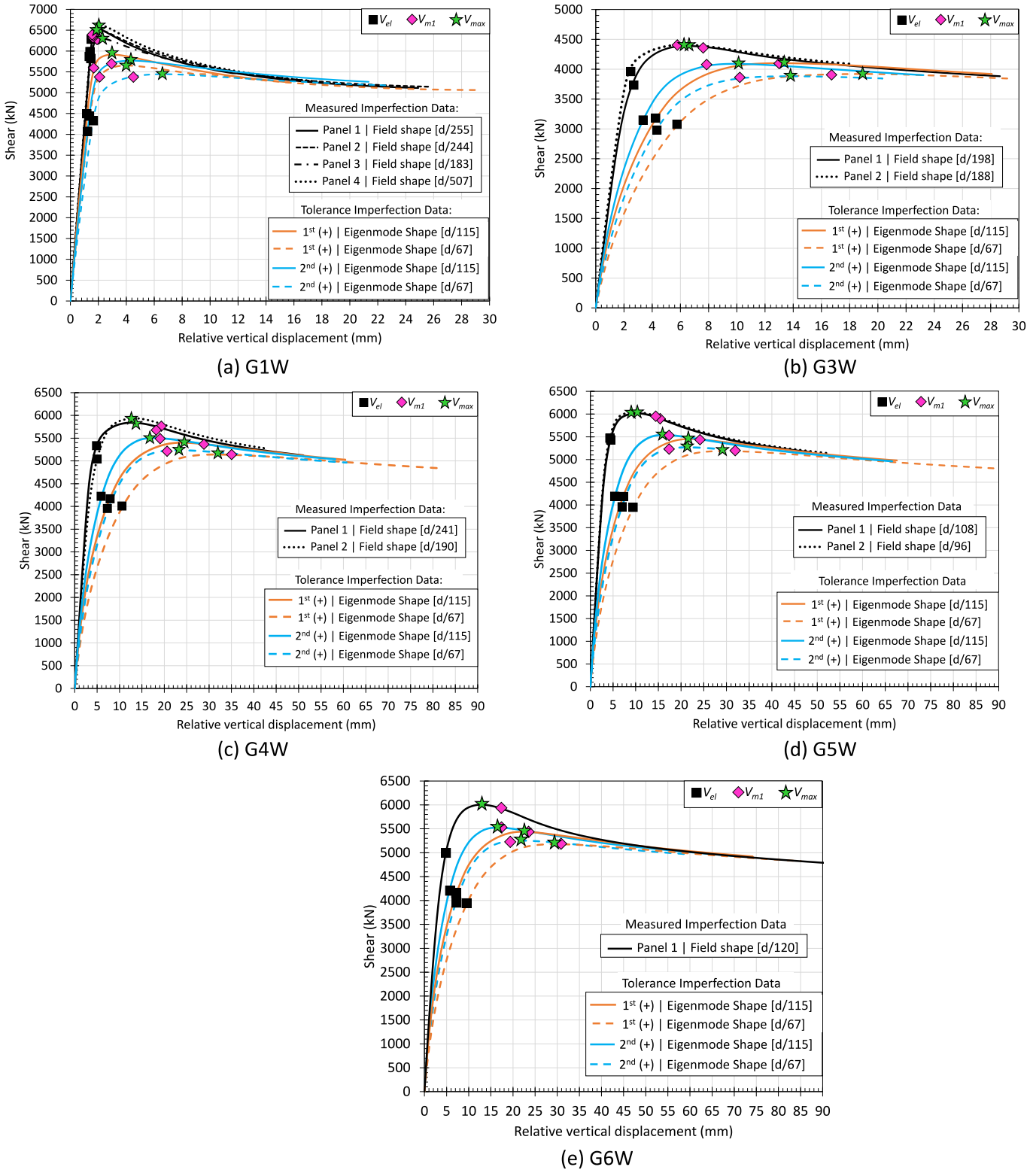

Fig. 6. FE results of various field measured and tolerance limit initial imperfections: shear load versus relative vertical displacements.

4. Numerical analysis results

Using the methodology and parameters described in Section 3, the effects of initial imperfection maximum magnitude and shape are examined numerically in this section.

4.1. Shear mechanism strength results

This section examines V_{el}, V_{m1}, V_{max} and the associated modes of shear mechanism response based on two parameters: *initial imperfection shape* (using field measured contours or eigenmodes) and *magnitude* (using field measured values or code limits). Table 2 includes all values for V_{el}, V_{m1}, and V_{max} from the FE model results (the approach to obtain these values followed the description discussed in Section 2 and 3.2) as well as code-based shear strength approximations per Chapter G of AISC [47] and Section 5 of EC3, Part 1–5 [18]. The nominal shear strength approximations per AISC with and without tension field action (TFA), and per EC3 pertains to the design of steel plate girders. It is important to note that code-based predictions do not explicitly consider sensitivities to initial imperfection magnitude and shape.

The shear load-displacement for all models with field measured imperfections (shape and magnitude) and the tolerance limit imperfections (with first or second positive eigenmode shapes) per Table 2 are plotted in Fig. 6. The results in Fig. 6 and Table 2 show smaller V_{m1} and V_{max} values for models with eigenmode shapes compared to models with field measured shapes. In addition, it is observed that V_{m1} and V_{max} values decrease when the maximum initial imperfection magnitude is increased. When V_{m1} is reached, very little to no stiffness remains in the web plate. At V_{max}, the shear stiffness is zero; and beyond V_{max}, the shear stiffness is negative, highlighting a redistribution of the load path. This trend correlates with similar observations made in previous research by others [11,12,14,28,48–51].

Examining the stiffness, the tolerance imperfection data set has a smaller stiffness than the measured imperfection data set due to the differences in initial imperfection shapes (as will be discussed next). Girder G1W (Fig. 6(a)) has $a/D = 0.89$, whereas the other plate girder a/D values range from 2.02 to 2.29 (Figs. 6(b-e)). As a result, the G1W FE results exhibit a larger initial shear stiffness response than the other plate girders, especially during the elastic behavior stage 1.

4.2. Direct comparisons of initial imperfection shape and magnitude

The measured imperfection data set has different initial imperfection shapes and magnitudes than the tolerance imperfection data set (Table 2); in other words, two parameters are varied at the same time thus the effects of shape and magnitude cannot be isolated. Therefore, plate girders G1W and G3W were used to directly evaluate the influence of initial imperfection shape and magnitude using a few variations of the measured and tolerance imperfection sets as listed in Table 3. The data marked with an asterisk is data that supplements Table 2. This additional data enables (1) an evaluation of the imperfection shape effect (by holding the magnitude constant), (2) an evaluation of the imperfection magnitude effect (by holding the shape constant), and (3) an estimation of a 'rounded' magnitude (with eigenmode shape) that can approximate the field measured results for purposes of future studies.

Fig. 7 plots the shear load versus relative vertical displacement of girder G1W and G3W with their respective imperfection magnitudes (one representing a tolerance limit of $d/67$ and the other a measured value of $d/183$ and $d/198$) and different imperfection shapes (field and first positive eigenmode). As expected, Fig. 7a and b shows that the shear load-displacement response becomes progressively stiffer and achieves slightly higher values of V_{el}, V_{m1}, and V_{max} when the maximum imperfection magnitude decreases (while holding the imperfection shape constant). This result is seen for both initial imperfection shapes (field and eigenmode). Specifically, Table 3 shows that the values of the shear milestones (V_{m1} and V_{max}) increase by 8% to 12% from $d/67$ to $d/183$ for field and eigenmode imperfection shapes when $a/D = 0.89$. When $a/D = 2.02$, the shear milestone values increase by 2% to 7% from $d/67$ to $d/188$.

The FE model with the field imperfection shape scaled to a very small maximum initial magnitude of $d/7000$ shows 7% increase in V_{max} for a/D=0.89, and a 2% increase for $a/D = 2.02$ when compared with the field measured imperfection magnitudes. Larger initial imperfection magnitudes enable an earlier onset of significant second-order bending over the in-plane compression diagonal, thus decreases, and varies the shear stiffness response of the web panel.

The imperfection magnitudes were scaled beyond the field and tolerance values to arrive at a value where eigenmode shapes can approximate the response of field imperfections. These scaling values were rounded for simplicity. From Table 3, it is seen that scaling the initial imperfection magnitude between $d/300$ to $d/600$ using the first

Table 3
Data of additional analyses for isolating the effect of initial imperfection shape and magnitude.

Plate Girder	Imp. Shape	Imperfection Magnitude		V_{el} (kN)	V_{m1} (kN)	V_{max} (kN)	$\frac{V_{m1}}{V_{m1}^{(**)}}$	$\frac{V_{max}}{V_{max}^{(**)}}$
		Value	[Basis]					
G1W	Field	**$d/183$**	**[field**]**	**5852**	**6297****	**6305****	**1.00**	**1.00**
($a/D = 0.89$, $D/t_w = 93$)	Panel 3	$d/67$*	[tolerance]	5266	5516	5521	0.88	0.88
		$d/7000$*	[very small]	6599	6725	6726	1.07	1.07
	1st (+) Eigen.	$d/67$	[tolerance]	4080	5490	5652	0.87	0.90
		$d/115$	[tolerance]	4508	5795	5914	0.92	0.94
		$d/183$*	[field]	5037	6151	6178	0.98	0.98
		$d/300$*	[rounded]	5365	6320	6326	1.00	1.00
		$d/400$*	[rounded]	5592	6425	6425	1.02	1.02
		$d/500$*	[rounded]	5802	6365	6523	1.01	1.03
G3W	Field	**$d/188$**	**[field**]**	**4293**	**4408****	**4408****	**1.00**	**1.00**
($a/D = 2.02$, $D/t_w = 118$)	Panel 2	$d/67$*	[tolerance]	4029	4277	4322	0.97	0.98
		$d/7000$*	[very small]	4226	4479	4483	1.02	1.02
	1st (+) Eigen.	$d/67$	[tolerance]	3083	3919	3920	0.89	0.89
		$d/115$	[tolerance]	3181	4102	4102	0.93	0.93
		$d/188$*	[field]	3578	4217	4227	0.96	0.96
		$d/300$*	[rounded]	3752	4301	4311	0.98	0.98
		$d/400$*	[rounded]	3827	4341	4349	0.98	0.99
		$d/500$*	[rounded]	3913	4367	4373	0.99	0.99
		$d/600$*	[rounded]	3945	4384	4390	0.99	1.00

[Basis] = the basis (source or reasoning) for the imperfection magnitude value
* = data added (not in Table 2) and used for further comparison purposes
** = data used for the denominator in the last two columns

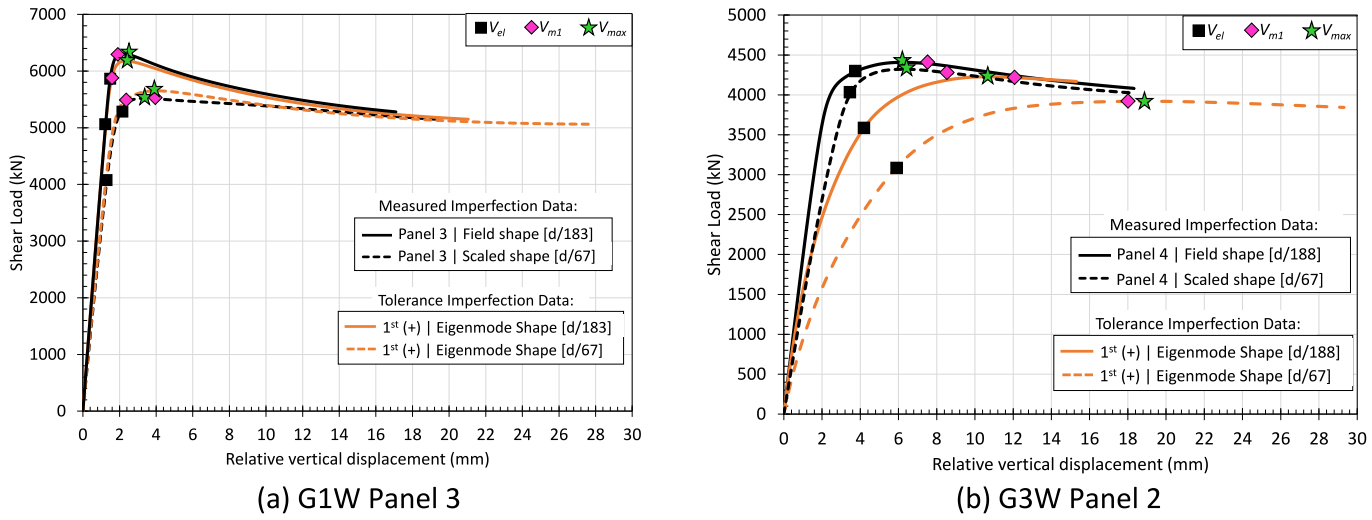

Fig. 7. Results for the panel extension FE models for (a) G1W ($a/D = 0.89$) and (b) G3W ($a/D = 2.02$).

positive eigenmode shape reliably captures V_{m1} and V_{max} within 3% to best match the shear strength results of field measured imperfections.

The G1W panel 3 and G3W panel 2 were examined with constant initial imperfection magnitudes of $d/183$ and $d/188$, respectively; and different initial imperfection shapes: field measured and eigenmode. Contours of the out-of-plane deformations are plotted in Fig. 8, which shows that the out-of-plane deformations of the web panels during the elastic, web mechanism, and panel mechanism stage will develop in onset deformations progressively irrespective of the initial imperfection shape (field measured or eigenmode). Therefore, these results indicate that the web essentially finds the same modes of postbuckling response regardless of the initial imperfection shape. But first, the field measured imperfection must be "pushed out" of its irregular initial shape into a deformed shape that more closely resembles the eigenmode. This transition enables a slightly greater initial shear stiffness (see Fig. 7b).

The same comparison evaluated the von Mises stresses plotted in Fig. 9 and Fig. 10 for the G1W web panel 3 and G3W panel 2 with the field measured and first eigenmode imperfection shapes scaled to the $d/183$ and $d/198$ maximum magnitudes, respectively. The von Mises stresses show that there is a variation in the development of the yield saturation surface due to the initial imperfection shape. While the eigenmode stress patterns are smoother than the field measured stress patterns, they both exhibit the same mechanism at the marked limit state. Although not shown, this behavior is observed for all web panels presented in this study.

Fig. 11 shows the values of V_{el}, and V_{m1} normalized by their respective V_{max} for each model in Table 2 and Table 3. The results are plotted as a function of their initial imperfection maximum magnitude. Cases with imperfection magnitude of $d/7000$ are omitted from the plotted data since the plot is intended to represent more realistic imperfection values. Additional models beyond those listed in Table 2 and Table 3 were analyzed to 'fill in' the gaps in the plotted data by applying a wider range of initial imperfection magnitude to several shape iterations of the G1W panel 3 and G3W panel 2 models. In Fig. 11a, V_{el}/V_{max} for field measured imperfection shapes are always larger than that of eigenmode imperfection shapes. Irrespective of the imperfection shape or magnitude, V_{el} is always reached at >70% of V_{max}. The ratios of V_{m1}/V_{max} in Fig. 11b reached ≥97% of V_{max} for all model cases.

4.3. Comparison with code-based predictions

The shear capacity obtained from the FE results is compared against code-based nominal shear strength predictions per AISC and EC3 [18,30]. In Table 2 and per AISC Chapter G specifications [30], V_n denotes the calculated nominal shear strength of webs for I-shaped members not considering tension field action (without TFA), which is based on a simplified implementation of Höglund's rotated stress theory [6]. $V_{n,TFA}$ represents the calculated nominal shear strength of web panels, which is based on Basler's full TFA theory per AISC Chapter G, section G2 [9]. $V_{bw,Rd}$ and $V_{b,Rd}$ represent the nominal shear strength calculated without and with the flange contributions respectively as prescribed by EC3 [18].

The value of V_{max} from each model is normalized by its corresponding code-based shear strength predictions and plotted in Fig. 12 and Fig. 13 as a bar graph results. These results include the measured and tolerance imperfections. The bar graphs can be interpreted as follows: if the ratio of V_{max}/code-based shear strength is <1.0, the code overestimates V_{max} and is thus unconservative.

The results show that AISC approximations without and with Tension Field Action (TFA) tend to overestimate the shear capacity for web panels with $a/D = 0.89$ by margins of 12% to 21% for the cases with tolerance imperfections, as demonstrated via the G1W plate girder ($a/D = 0.89$) models. For model cases with measured imperfections, AISC also overestimates V_{max} by margins of 1% to 9% where $a/D = 0.89$. For girder webs with $a/D \geq 2.0$ as shown in Fig. 13 (G3W, G4W, G5W, and G6W), AISC without TFA tends to underestimate V_{max} for cases with both measured and tolerance imperfections by margins of 6% to 28%. For cases with TFA, AISC can conservatively underestimate V_{max} by margins of 13% to 15% for measured imperfections, and 1% to 6% for cases with tolerance imperfections.

At the upper bound tolerance imperfection limit of $d/67$, both AISC with TFA and EC3 with flange contributions tend to overestimate V_{max} by margins of 1% to 3%. The EC3 shear strength approximations with and without the contribution of flanges conservatively underestimate V_{max} by margins of 1% to 22% for model cases with measured imperfections. In contrast, the EC3 approach tends to overestimate V_{max} by ranges of 1% to 10% for model cases with tolerance imperfections. In general, the EC3 approximations tend to yield conservative shear strength predictions when not considering the contribution of the flanges.

5. Conclusions

This study numerically evaluated the influence of initial imperfection magnitude and shape on the shear behavior and strength of I-shaped steel plate girder webs. Specifically, two categories of imperfections were considered: (1) measured imperfection shapes and magnitudes as

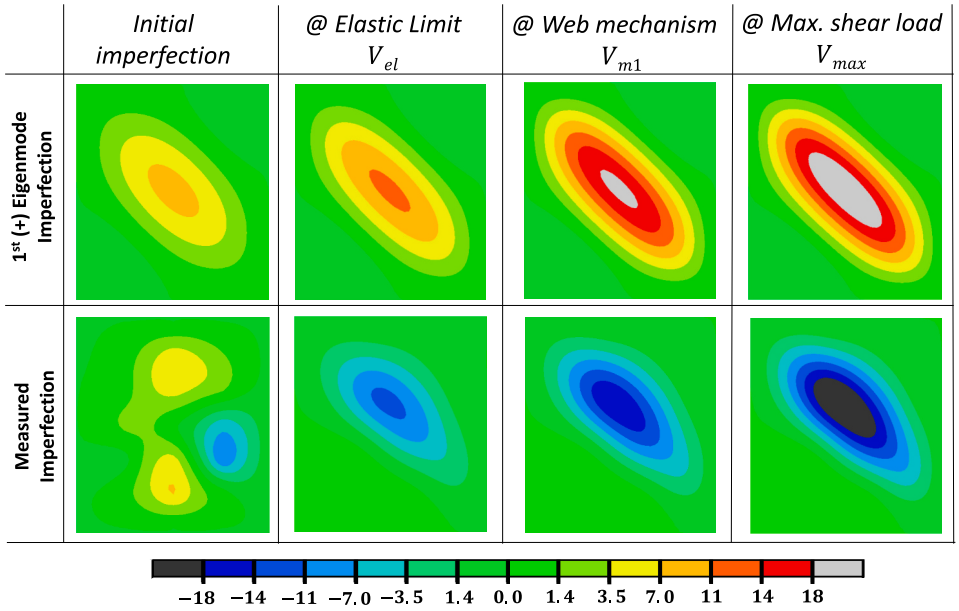

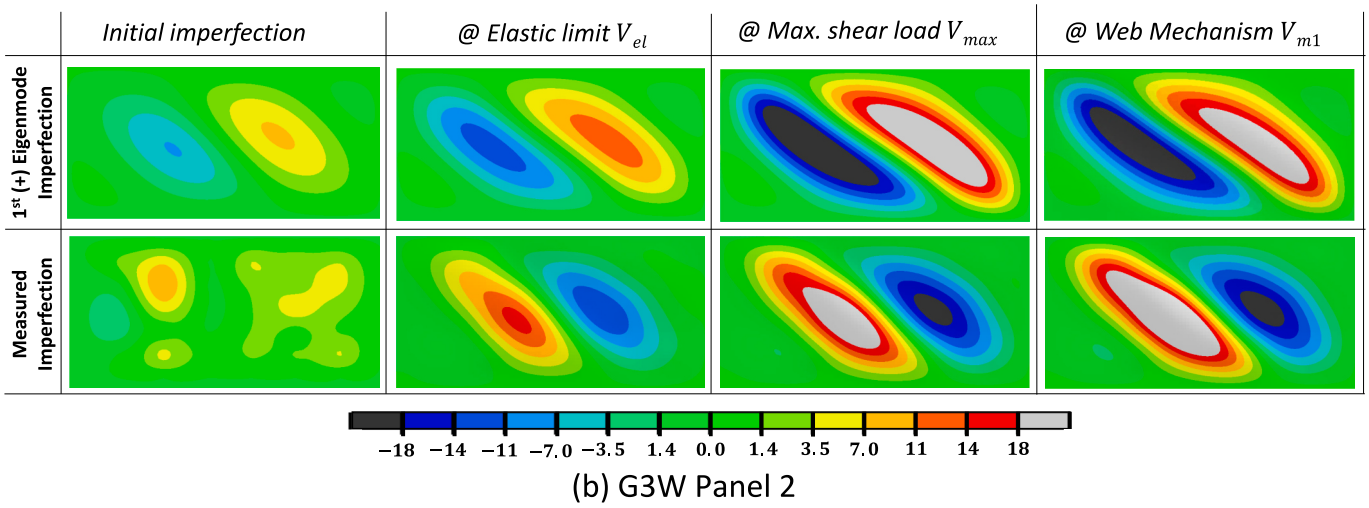

Fig. 8. Contours of out-of-plane deformations (*mm*) from FE analyses: (a) G1W panel 3 ($d/183$) and (b) G3W panel 2 ($d/188$)

measured in the field from recently fabricated bridge girders, and (2) eigenmode imperfection shapes with maximum magnitudes in accordance with code-based tolerance limits as prescribed by the bridge welding code, AASHTO/AWS D1.5 [17]. Finite element (FE) models were used to parametrically examine the shear mechanism response, the surface and through-thickness yield mechanism milestones (V_{el}, V_{m1}), and the maximum shear capacity (V_{max}). The following conclusions can be drawn from the results of this study:

- The field measured and tolerance imperfection data exhibit similar shear behavior and deformation response during all shear mechanism stages.
- At large initial imperfection magnitudes, field measured imperfection models exhibit slightly larger stiffness and V_{max} in comparison to those with code-based tolerance imperfections. As observed by other investigators [11,12,28,48,49,52], larger initial imperfection magnitudes lead to a decrease in V_{max}.
- Based on the web out-of-flatness geometry (shapes and magnitudes) captured in the field study, the numerical shear strength results reveal that scaling the first positive eigenmode shape to a maximum rounded magnitude ranging between $d/300$ and $d/600$ can produce nearly the same V_{max} value similar to models using field imperfections.
- The FE results with web panel sections where the aspect ratio (a/D) is 0.89 exhibited a larger initial shear stiffness response than web panel sections where $a/D \geq 2.0$ during the elastic behavior stage 1 and the web mechanism stage 2.
- The commonly adopted eigenmode buckled shapes employed in the literature are indeed conservative bottom lines when compared to real field measured imperfection shapes.
- Current code-based shear strength formulations are inconsistently conservative versus the results of FE models that utilize a broad range of initial imperfection shapes and magnitudes.

The numerical modeling approaches demonstrated in this study can be used to develop improved code-based equations for the nominal shear strength of slender web plates, thus enhancing the prediction of the maximum shear capacity of I-shaped plate girders. Further studies of different plate girder geometries beyond those presented here would help generalize the conclusions of this paper.

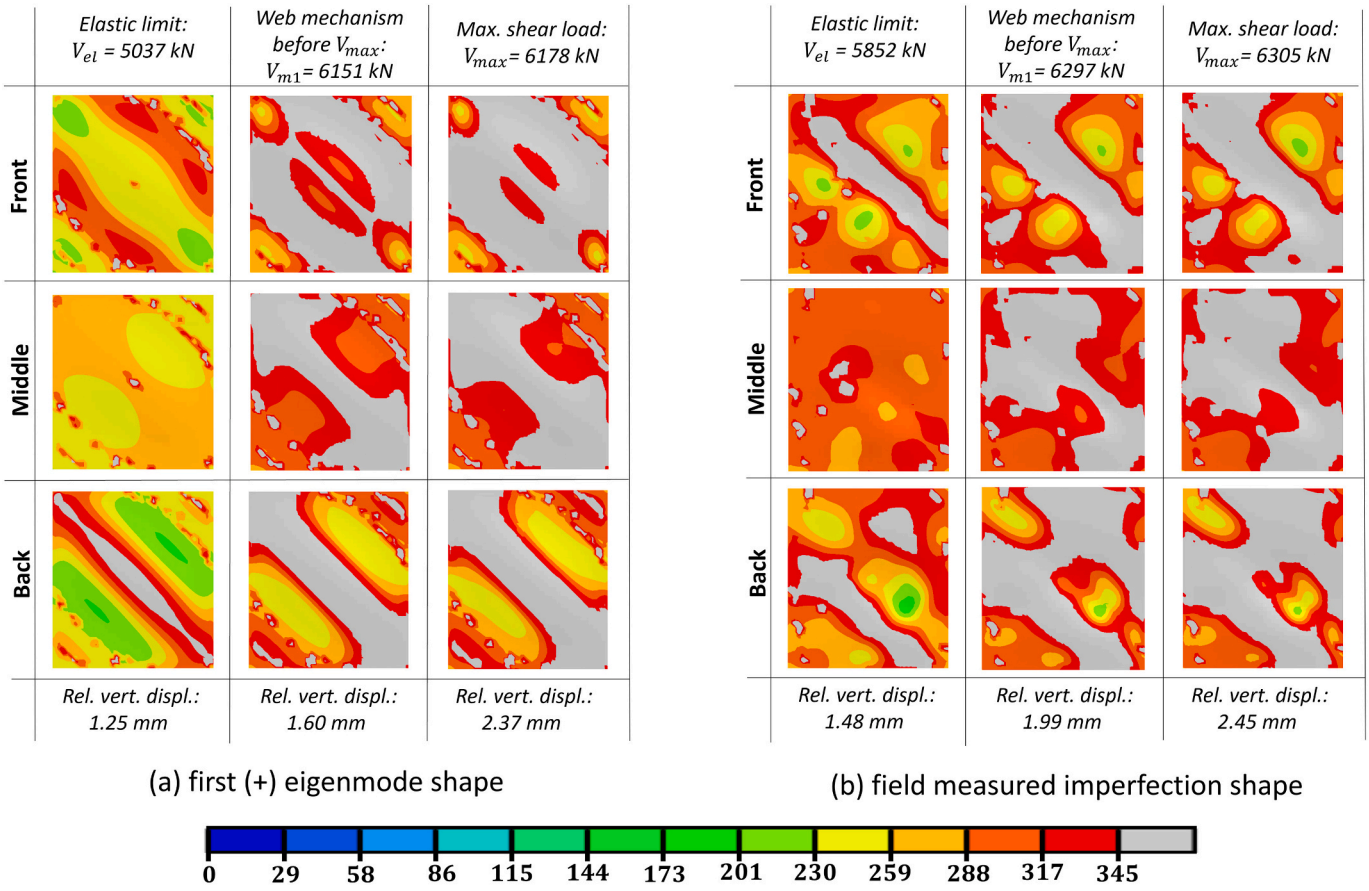

Fig. 9. Contours of von Mises stresses (*MPa*) at surface and mid-thickness integration points for G1W web panel 3 ($a/D = 0.89$) at several shear milestones. Maximum initial imperfection magnitude = $d/183$.

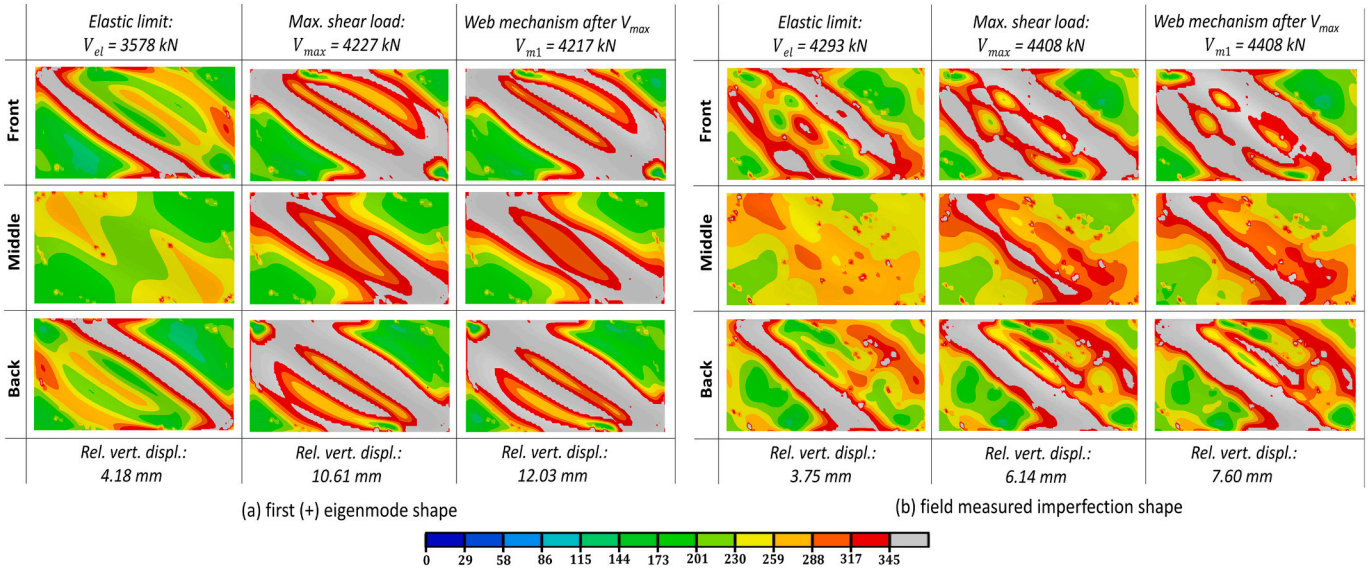

Fig. 10. Contours of von Mises stresses (*MPa*) at surface and mid-thickness integration points for G3W web panel 2 ($a/D = 2.02$) at several shear milestones. Maximum initial imperfection magnitude = $d/188$.

CRediT authorship contribution statement

Parfait M. Masungi: Writing – review & editing, Writing – original draft, Visualization, Validation, Supervision, Software, Resources, Project administration, Methodology, Investigation, Formal analysis, Data curation, Conceptualization. **Maria E.M. Garlock:** Writing – review & editing, Visualization, Supervision, Resources, Project administration, Methodology, Funding acquisition, Formal analysis, Conceptualization. **Kevin E. Augustyn:** Project administration, Methodology, Investigation, Data curation, Conceptualization. **Spencer E.**

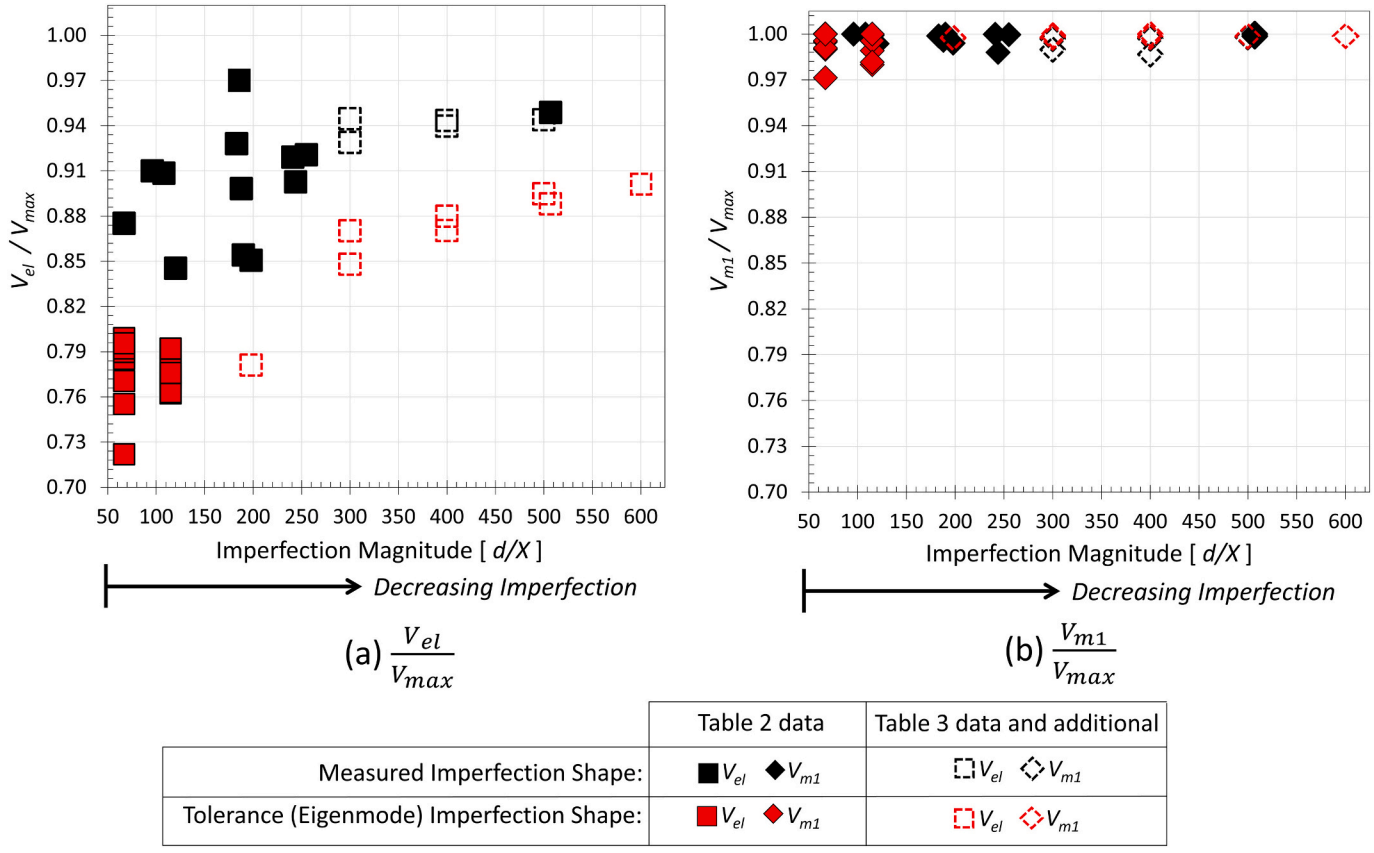

	Table 2 data	Table 3 data and additional
Measured Imperfection Shape:	V_{el} V_{m1}	V_{el} V_{m1}
Tolerance (Eigenmode) Imperfection Shape:	V_{el} V_{m1}	V_{el} V_{m1}

Fig. 11. Relationship of shear milestones (normalized by V_{max}) versus maximum imperfection magnitude. G1W web panel 3 and G3W web panel 2 were used to develop the additional scaled imperfection data.

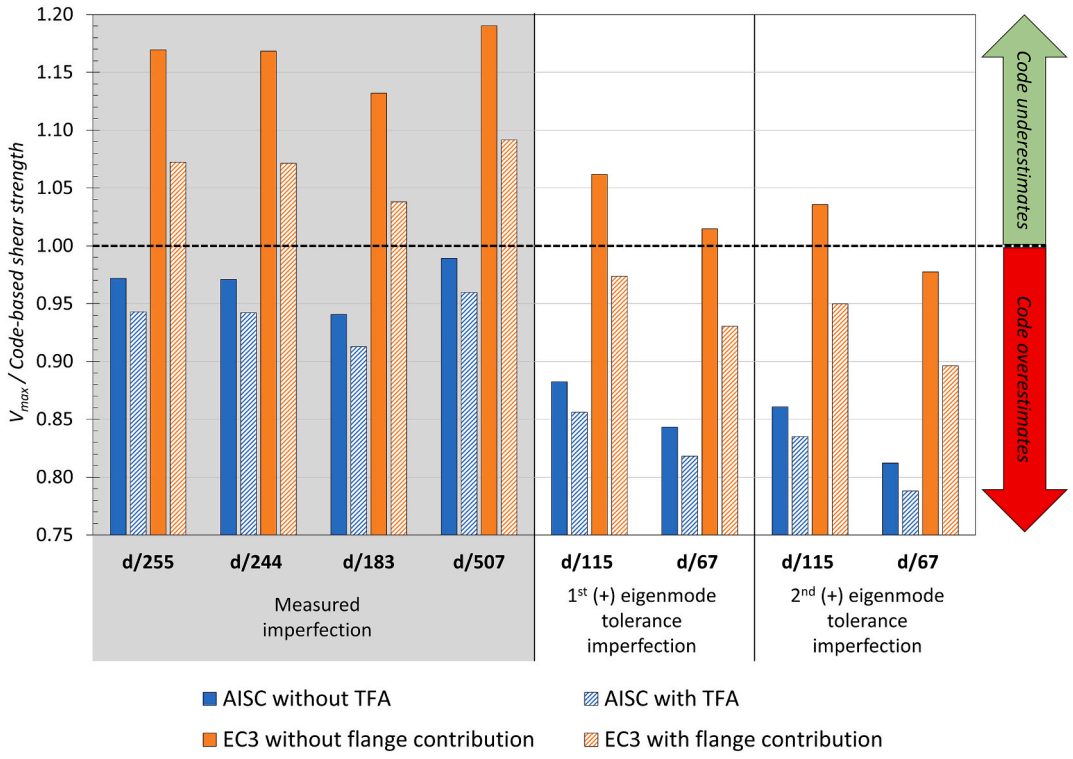

Fig. 12. Comparison of FE V_{max} results against code-based shear strength approximations for G1W (a/D=0.89).

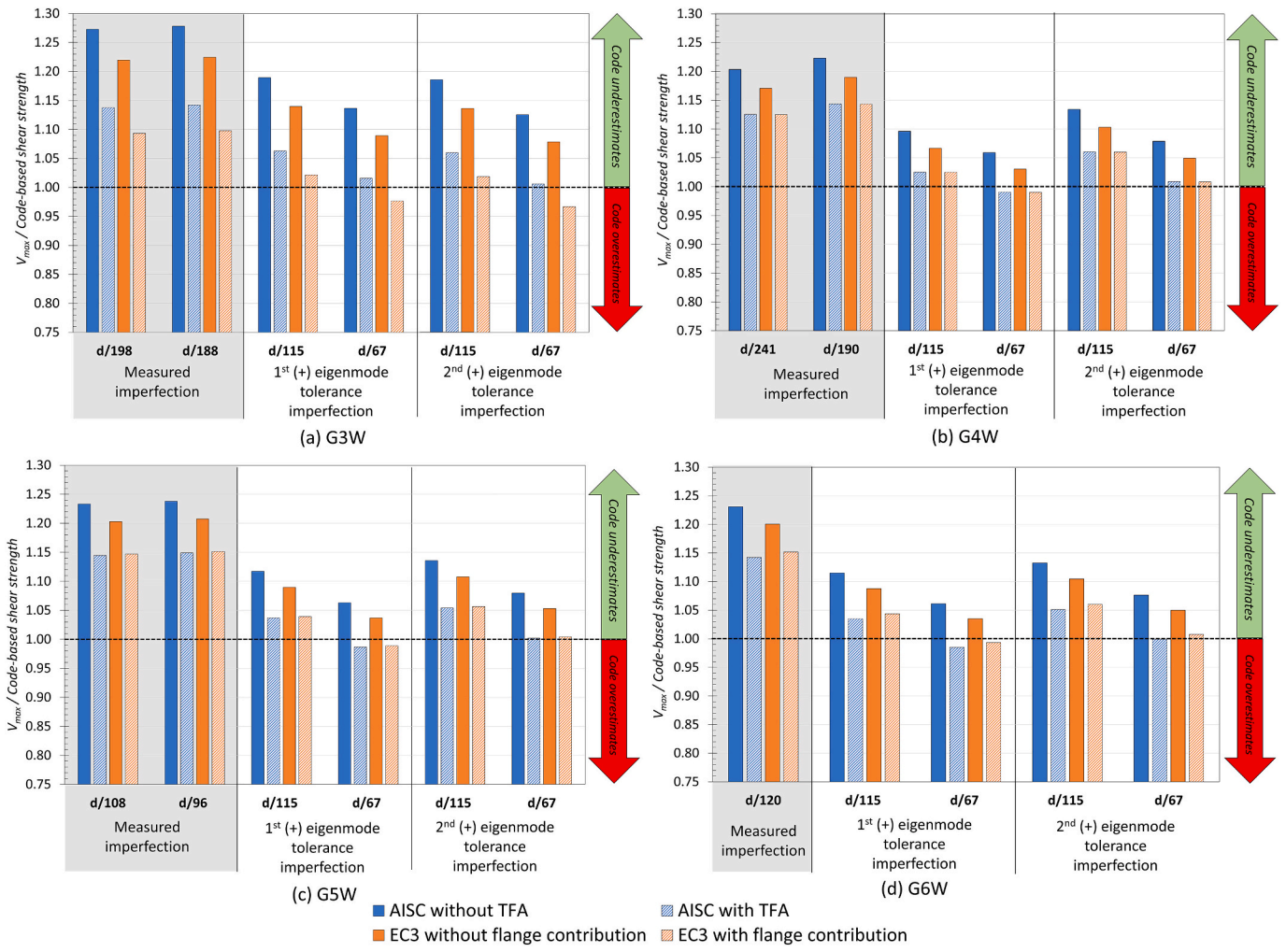

Fig. 13. Comparison of FE V_{max} results against code-based shear strength approximations for G3W, G4W, G5W, and G6W ($a/D \geq 2.0$).

Quiel: Writing – review & editing, Validation, Resources, Project administration, Methodology, Funding acquisition, Conceptualization.

Declaration of competing interest

The authors declare that they have no known competing financial interests or personal relationships that could have appeared to influence the research study and work reported in this paper.

Data availability

Data will be made available on request.

Acknowledgments

The research was sponsored by the National Science Foundation (NSF) under Grants CMMI-1662886 and CMMI-1662964. All opinions expressed in this paper are of the authors and do not necessarily reflect the policies and views of NSF. The authors would like to thank Peter Y. Wang for his valuable perspective; and Ronnie Medlock at High Steel, LLC for his support, consultation, and collaboration in facilitating the accomplishment of the companion work presented in Part I [4].

References

[1] J.M. Wilson, On specifications for strength of iron bridges, Trans. Am. Soc. Civ. Eng. 15 (1886) 389–414, https://doi.org/10.1061/taceat.0000597.
[2] Y.D. Kim, D.W. White, Transverse stiffener requirements to develop shear-buckling and postbuckling resistance of steel I-girders, J. Struct. Eng. 140 (2014) 04013098, doi:10.1061.
[3] F. Bleich, Buckling Strength of Metal Structures, McGraw-Hill, New York, 1952. https://www.worldcat.org/title/buckling-strength-of-metal-structures/oclc/1578095 (accessed April 3, 2021).
[4] P.M. Masungi, M.E.M. Garlock, S.E. Quiel, Out-of-flatness of steel plate girder webs, part I: tolerance review and measurements, J. Constr. Steel Res. 215 (2024).
[5] K. Basler, Strength of plate girders under combined bending and shear, J. Struct. Eng. ASCE 87 (1961) 181–197. http://preserve.lehigh.edu/engr-civil-environmental-fritz-lab-reports/71.
[6] T. Höglund, Shear buckling resistance of steel and aluminium plate girders, Thin-Walled Struct. 29 (1997) 13–30, https://doi.org/10.1016/s0263-8231(97)00012-8.
[7] D.M. Porter, K.C. Rockey, H.R. Evans, The collapse behaviour of plate girders loaded in shear, Struct. Eng. J. 53 (1975) 313–325.
[8] C.H. Yoo, S.C. Lee, D.S. Lee, Mechanics of web panel postbuckling behavior in shear, J. Struct. Eng. 132 (2006) 1582–1589, https://doi.org/10.1061/(asce)0733-9445(2006)132:10(1580).
[9] K. Basler, Strength of plate girders in shear, J. Struct. Div. 87 (1961) 151–180. https://ascelibrary.org/doi/epdf/10.1061/JSDEAG.0000697.
[10] Y. Zhang, Strength Based Plate Tolerances for Steel Bridge Girders, University of Houston, 2007. https://www.proquest.com/docview/304848549/fulltextPDF/8DADE31680E94B9BPQ/1?accountid=13314.
[11] N. Rangelov, A theoretical approach to the limiting of initial imperfections in steel plates, Stahlbau 61 (1992) 151–156.
[12] S. Komatsu, Y. Niwa, E. Watanabe, Statistical study on imperfections of steel webs, J. Struct. Eng. 109 (1983) 419–438, https://doi.org/10.1061/(ASCE)0733-9445(1983)109:2(419).
[13] A. Ghadami, V. Broujerdian, Shear behavior of steel plate girders considering variations in geometrical properties, J. Constr. Steel Res. (2019) 567–577, https://doi.org/10.1016/j.jcsr.2018.11.009.
[14] P.Y. Wang, P.M. Masungi, M.E.M. Garlock, S.E. Quiel, Postbuckling mechanics in slender steel plates under pure shear: a focus on boundary conditions and load

path, Thin-Walled Struct. 169 (2021), https://doi.org/10.1016/j.tws.2021.108448.
[15] Bridge Welding Code, Foreword: AASHTO/AWS D1.5M/D1.5:2002, 2002.
[16] American Welding Society, AWS D2.0–66, Specifications for Welded Highway and Railway Bridges, 1966.
[17] AASHTO/AWS D1.5M/D1.5, Bridge Welding Code, 8th edition, American Welding Society, United States of America, 2020.
[18] European Committee for Standardization, CEN 1993-1-5, Eurocode 3: Design of Steel Structures: Plated Structural Elements, Brussels, 2006.
[19] AS/NZS 3678:2016, Structural Steel—Hot-Rolled Plates, Floorplates and Slabs, 4th Editio, Australian/New Zealand Standard, 2016.
[20] BS 5400-9-1:1983 Steel, concrete and composite bridges. Bridge bearings. Code of practice for design of bridge bearings, British Standards Institution, London, UK, 1983. https://www.thenbs.com/PublicationIndex/documents/details?Pub=BSI&DocID=280619 (accessed June 28, 2022).
[21] Deutscher Ausschuss für Stahlbau, DASt-Richtlinie 012: Beulsicherheitsnachweise für Platten, 1980.
[22] JHSB, Specifications for Highway Bridges: Part II Steel Bridges, Japan Road Association, Tokyo, Japan, 1973.
[23] European Recommendations for Steel Construction, Code: 023. https://store.steelconstruct.com/site/index.php?module=store&target=publicStore&id_category=2&id=104, 1978 (accessed June 28, 2022).
[24] Introduction à la nouvelle norme SIA 161, 1979. https://books.google.com/books?id=TDpavgAACAAJ, 1979.
[25] Stalen Bouwconstructies, NBN B 51–001 - Belgian Institute for Standardisation, Belgische norm, https://books.google.com/books/about/Stalen_bouwconstructies_NBN_B_51_001.html?id=qAMQrgEACAAJ, 1977.
[26] Standards Australia, Australian Steel Institute - AS 1250–1981 SAA Steel Structures Code. https://www.steel.org.au/resources/elibrary/library/as-1250-1981-saa-steel-structures-code/, 1981.
[27] A. Bergfelt, Patch Loading on a Slender Web-Influence of Horizontal and Vertical Stiffeners on the Load Carrying Capacity, Chalmers University of Technology, 1979.
[28] S.C. Lee, C.H. Yoo, Strength of plate girder web panels under pure shear, J. Struct. Eng. 124 (2) (1998) 184–194.
[29] A. Ghadami, V. Broujerdian, Flexure–shear interaction in hybrid steel I-girders at ambient and elevated temperatures, Adv. Struct. Eng. 22 (2019) 1501–1516, https://doi.org/10.1177/1369433218817893.
[30] American Institute of Steel Construction, AISC 360–22 Specification for Structural Steel Buildings, 2022.
[31] K.E. Augustyn, S.E. Quiel, M.E.M. Garlock, Formation of post-buckling shear mechanisms in stiffened web panels of slender steel plate girders, Thin-Walled Struct. 184 (2023) 110481, https://doi.org/10.1016/J.TWS.2022.110481.
[32] D.R. Hingnekar, A.Y. Vyavahare, Mechanics of shear resistance in steel plate girder: critical review, J. Struct. Eng. 146 (2020), https://doi.org/10.1061/(ASCE)ST.1943-541X.0002484.
[33] D.W. White, M.G. Barker, Shear resistance of transversely stiffened steel I-girders, J. Struct. Eng. 134 (2008) 1425–1436, https://doi.org/10.1061/(asce)0733-9445(2008)134:9(1425).
[34] J.D. Glassman, M.E.M. Garlock, Compression Model for Ultimate Postbuckling Shear Strength at Elevated Temperatures, J. Struct. Eng. (United States). 143 (2017) 1–11, https://doi.org/10.1061/(ASCE)ST.1943-541X.0001737.
[35] A.W. Davies, D.S.C. Griffith, Shear strength of steel plate girders, Proc. Inst. Civ. Eng. Struct. Build. 134 (1999) 147–157, https://doi.org/10.1680/ISTBU.1999.31381.
[36] K.C. Rockey, M. Skaloud, The ultimate load behaviour of plate girders loaded in shear, Struct. Eng. 50 (1972) 29–48.
[37] C. Scandella, M. Neuenschwander, K.M. Mosalam, M. Knobloch, M. Fontana, Structural behavior of steel-plate girders in shear : experimental study and review of current design principles, J. Struct. Eng. 146 (2020) 1–16, https://doi.org/10.1061/(ASCE)ST.1943-541X.0002804.
[38] K.E. Augustyn, S.E. Quiel, M.E.M. Garlock, Post-buckling shear resistance of slender girder webs : stiffener participation and flange contributions, J. Constr. Steel Res. 190 (2022) 107117, https://doi.org/10.1016/j.jcsr.2021.107117.
[39] S.C. Lee, C.H. Yoo, Experimental study on ultimate shear strength of web panels, J. Struct. Eng. 125 (1999) 838–846.
[40] S.C. Lee, M. Asce, H. Yoo Chai, D.Y. Yoon, Behavior of Intermediate Transverse Stiffeners Attached on Web Panels, J. Struct. Eng. 128 (2002) 337–345, https://doi.org/10.1061/(ASCE)0733-9445(2002)128:3(337.
[41] S.C. Lee, D.S. Lee, C.H. Yoo, Further insights into postbuckling of web panels. I: Review of Flange anchoring mechanism, J. Struct. Eng. 135 (2009) 3–10, https://doi.org/10.1061/(ASCE)0733-9445(2009)135:1(11.
[42] C.H. Yoo, S.C. Lee, Mechanics of web panel postbuckling behavior in shear, J. Struct. Eng. 132 (2006) 1580–1589, https://doi.org/10.1061/(asce)0733-9445(2006)132:10(1580).
[43] K.E. Augustyn, S.E. Quiel, M.E.M. Garlock, Post-buckling shear resistance of slender girder webs: stiffener participation and flange contributions, J. Constr. Steel Res. 190 (2022) 107117, https://doi.org/10.1016/J.JCSR.2021.107117.
[44] Abaqus: Analysis User's Guide, Version 2022, Dassault Systèmes Simulia, USA, 2022.
[45] Eurocode 3, Design of Steel Structures-Part 1–2: General Rules-Structural Fire Design, London. http://www.nsai.iesaleshttp//www.standards.ie, 2001.
[46] P.Y. Wang, K.E. Augustyn, A. Gomez, S.E. Quiel, M.E.M. Garlock, Influence of boundary conditions on the shear post-buckling behavior of thin web plates, in: SSRC Annu. Stab. Conf., Structural Stability Research Council (SSRC), Saint Louis, MO, 2019 doi:10.2/JQUERY.MIN.JS.
[47] AISC, Steel Construction Manual: Specification for Structural Steel Buildings (ANSI/AISC 360–16) | Code of Standard Practice for Steel Buildings and Bridges, 15th edition, United States of America, 2017. https://www.aisc.org/Specification-for-Structural-Steel-Buildings-ANSIAISC-360-16-1.
[48] P.J. Dowling, P.A. Frieze, J.E. Harding, Imperfection Sensitivity of Steel Plates under Complex Edge Loading, Second International Colloquium on Stability of Steel Structures, in: Second Int. Colloq. Stab. Steel Struct., Stability of Steel Structures, Liege, 1977, pp. 305–314.
[49] Z. Sadovský, I. Baláž, Tolerances of initial deflections of steel plates and strength of I cross-section in compression and bending, J. Constr. Steel Res. 38 (1996) 219–238, https://doi.org/10.1016/0143-974X(96)00020-X.
[50] A. Gomez, Web out-of-Straightness in Plate Girders: Methodology for Measurements and Effects on Shear Capacity, Princeton University, USA, 2020.
[51] Z. Kala, J. Kala, M. Škaloud, B. Teplý, Sensitivity analysis of the effect of initial imperfections on the (i) ultimate load and (ii) fatigue behaviour of steel plate girders, J. Civ. Eng. Manag. 11 (2005) 99–107, https://doi.org/10.1080/13923730.2005.9636338.
[52] E.G. Thimmhardy, R.M. Korol, Geometric imperfections and tolerances for steel box girder bridges, Can. J. Civ. Eng. 15 (1988) 437–442, https://doi.org/10.1139/L88-059.